Available online www.ejaet.com

European Journal of Advances in Engineering and Technology, 2017, 4(11): 866-877

Research Article ISSN: 2394 - 658X

Non Linear Thermal Radiation Effects on MHD Heat and Mass Transfer in Carreau Nanofluid Over a Permeable Stretching Sheet with Suction\Injection

Vijaya Bhaskar Reddy Nimma[1] and Kishan Naikoti[2]

[1]Government Degree College (Autonomous), Siddipet Dist., Telangana state, India
[2]Department of Mathematics, University College of Science,
Osmania University, Hyderabad, Telangana state, India
vijju.reddy20@gmail.com

ABSTRACT

The present paper deals with the flow, heat and mass transfer characteristics of magneto hydrodynamics in carreau nanofluid over a permeable stretching sheet with convective boundary conditions in the presence of non-linear thermal radiation and suction\injection effects. The non-linear partial differential equations that govern the flow were transformed to nonlinear ordinary differential equations by using similarity variables and solved numerically by employing Runge-Kutta technique along with shooting method. The numerical results are obtained to discuss the behaviour of velocity, temperature and nanoparticle volume fraction profiles for various parameters of interest were discussed and present through graphs. Also the numerical values of skin friction coefficient, local Nusselt and Sherwood numbers are tabulated.

Keywords: Carreau Nanofluid, MHD, Permiable Stretching sheet, Nonlinear thermal radiation, suction\injection

INTRODUCTION

Nanofluids are the materials that consist of small quantities of nano meter-size particles, known as nanoparticles. Typically, the nanoparticles are made of oxides like alumina, titania and copper oxide, carbides and metals including copper and gold. Diamond and Carbon nanotubes have also been utilized in nanofluids. These particles have ability to increase thermo physical properties of the base liquids. The base fluids include oil, ethylene glycol, water, bio fluids, polymer solutions and some lubricants. Choi [1] was the first one who introduced this colloidal suspension. Buongiorno [2] studied the convective transport phenomena in nanofluid. He constructed a mathematical model to study the nanofluid flow comprising Brownian motion and thermophoretic dispersion of nanoparticles. The two dimensional stretched flow of nanofluid is conducted by Khan and Pop [3]. Makinde and Aziz [4] extended this analysis by considering convective boundary conditions. They demonstrated that convective heating significantly affects the thermal boundary layer. Having such facts in mind, many engineers and scientists are busy in the investigations of flows of nanofluid via various aspects. Few representative studies in this direction can be seen in the attempts [5–10].

The range of non-Newtonian fluids is very large because of their presence in the engineering and industrial processes. Such fluids are quite commonly used in the manufacture of coated sheets, foods, optical fibres, drilling muds, plastic polymers, etc. It is well known that all the non-Newtonian fluids, because of their diverse characteristics, cannot be described by a single constitutive relationship. Hence several models of non-Newtonian fluids have been suggested. The governing equations for the flows of non- Newtonian fluids, in general, are much complicated, more nonlinear and of higher order than the Navier–Stokes equations. Unlike power-law fluid, the Carreau model is one of the non-Newtonian fluid models for which constitutive relationship holds at both low and high shear rates. Due to this fact, it has achieved wider acceptance at present. Hayat et al [11] investigated the boundary layer flow of Carreau fluid over a convectively heated stretching sheet. Ali and Hayat [12] discussed the peristaltic transport of Carreau fluid in an asymmetric channel. Heat and mass transfer in hydromagnetic flow of Carreau fluid past a vertical porous plate with thermal radiation and thermal diffusion is addressed by Olajuwon [13]. Tshehla [14] studied the flow of Carreau fluid down an inclined free surface.

The investigation of the magnetic field has critical reasonable applications in medical and engineering sciences. Numerous mechanical sorts of supplies, for example, pumps, bearing, MHD generators, and boundary layer flow control are influenced by the connection between a magnetic field and electrically conducting fluid. A. Malvandi et. a*l.* [15] studied is the behaviour of the flow firmly relies on upon the intensity and orientation force of the magnetic field. The essential finds out about MHD liquid flow was coordinated by Alfven *et al* [16] who won the Nobel Prize for his work. Sheikholeslami *et al* [17] analyzed the effect of magnetic field in the nanofluid flow in a porous channel. Jashim *et al* [18] demonstrated the mathematical modelling of MHD thermo solute nanofluid flow in porous medium under the influence of convection slip conditions.

Besides, the radiative heat transfer has wide occurrence in various applications, such as in nuclear power plants, gas turbines, propulsion devices for space vehicles, missiles and aircraft etc. In view of these applications, many researchers [19–23] have considered the influence of thermal radiation effect with different physical situations. To simplify the radiative heat, flux the Rosseland approximation has been employed. Further, they have assumed small temperature differences within the flow to make out the linear radiative heat flux. But in recent years, many authors have an interest in the study of non-linear thermal radiation effect (see [24–27]). However, aforementioned studies are restricted to linearly stretching sheet. It is important to note that in many practical applications, the stretching of the sheet is not necessarily linear. It may be quadratic, exponential or non-linear. Keeping this in view, the effects of various parameters on the two dimensional flow towards a nonlinearly stretching sheet have been studied by many authors [28-31].

For physical situations, the average behaviour of heat generation or absorption can be expressed by some simple mathematical models because its exact modelling is quite difficult. Heat generation or absorption has been assumed to be constant, space dependent, or temperature-dependent. Sparrow and Cess [32] investigated the steady stagnation point flow and heat transfer in the presence of temperature dependent heat absorption. Later, Azim *et al* [33] discussed the effect of viscous Joule heating on MHD-conjugate heat transfer for a vertical flat plate in the presence of heat generation. One of the latest works is the study of the heat transfer characteristic in the mixed convection flow of a nanofluid along a vertical plate with heat source/sink studied by Rana and Bhargava [34].

The suction or injection of a fluid flowing through a bounding surface can significantly change the flow field. Suction is applied to chemical processes to remove reactants, cool the surface, reduce the drag, prevents corrosion in the fluid. The injection of fluid finds applications in film cooling, polymer fiber coating, a coating of wires etc. Nayak [35] examined the influence of suction and injection on the velocity and temperature profiles in the second order and second-grade fluid flow past a stretching sheet. Hayat *et al* [36] described the influence of suction and injection on the MHD flow of nanofluid over a permeable stretching sheet in presence of convective boundary conditions. This investigation reveals that the increase in suction draws more amount of fluid particles into the sheet resulting a decrease in velocity field and the reverse effect is observed when the injection is applied to the fluid.

The present objective is to attempt a mathematical model of heat and mass transfer in carreau nanofluid flow over a permeable stretching sheet with convective slip conditions in the presence of magnetic field, heat source\sink and nonlinear thermal radiation. To achieve this study, the suitable transformation is used to transform the partial differential equations to a system of ordinary differential equations together with boundary conditions the resulting system of ordinary differential equations are solved using the well-known Runge-Kutta technique along with shooting method.

MATHEMATICAL FORMULATION

Let us consider the steady, two-dimensional boundary layer flow of an incompressible Carreau nanofluid bounded by a permeable stretching surface at $y = 0$. The x- and y-axes are taken parallel and transverse to the stretched surface. The fluid is considered as electrically conducting and a uniform magnetic field of strength B_0 applied in the x-direction. Non-linear thermal radiation along with heat source\sink effects is taken into account. Further, it is assumed that the magnetic Reynolds number is very small and so that the induced magnetic field is neglected. We are also considered the velocity, thermal and solutal slip conditions. It is assumed that the sheet is considered along x-axis with stretching velocity and y-axis is normal to it with the flow is confined to $y \geq 0$..The extra stress tensor for carreau fluid is given by

$$\tau_{ij} = \left[\eta_\infty + (\eta_{0-}\eta_\infty)[1 + (\Gamma\dot{\gamma})^2]^{\frac{n-1}{2}}\right]\dot{\gamma} \tag{1}$$

Where τ_{ij} is the extra stress tensor, η_0 is the zero shear rate viscosity, η_∞ is the infinity shear rate viscosity, λ is the time constant, n is the power law index and $\dot{\gamma}$ is defined as follows

$$\dot{\gamma} = \sqrt{\frac{1}{2}\sum_i\sum_j \dot{\gamma}_{ij}\dot{\gamma}_{ji}} = \sqrt{\frac{1}{2}\Pi} \tag{2}$$

Here Π is the second invariant of strain-rate tensor. We consider the constitutive equation when $\eta_\infty = 0$ so equation (1) becomes

$$\tau_{ij} = \left[\eta_0[1 + (\Gamma\dot{\gamma})^2]^{\frac{n-1}{2}}\right]\dot{\gamma} \tag{3}$$

Using equation (3) and the boundary layer equations governing the conservations of mass, momentum, energy and nanoparticle concentration for the Carreau nanofluid in the present flow consideration are

$$\frac{\partial u}{\partial x} + \frac{\partial v}{\partial y} = 0 \tag{4}$$

$$u\frac{\partial u}{\partial x} + v\frac{\partial u}{\partial x} = \nu\frac{\partial^2 u}{\partial y^2}\left[1 + \left(\frac{n-1}{2}\right)\lambda^2\left(\frac{\partial u}{\partial y}\right)^2\right] + \nu(n-1)\lambda^2\frac{\partial^2 u}{\partial y^2}\left(\frac{\partial u}{\partial y}\right)^2\left[1 + \left(\frac{n-3}{2}\right)\lambda^2\left(\frac{\partial u}{\partial y}\right)^2\right] - \frac{\sigma}{\rho}B_0^2 u = 0 \tag{5}$$

$$u\frac{\partial T}{\partial x} + v\frac{\partial T}{\partial y} = \alpha\frac{\partial^2 T}{\partial y^2} - \frac{1}{\rho c_p}\frac{\partial q_r}{\partial y} + \tau\left[D_B\frac{\partial C}{\partial y}\frac{\partial T}{\partial y} + \frac{D_T}{T_\infty}\left(\frac{\partial T}{\partial y}\right)^2\right] + \frac{Q_0}{(\rho c)_f}(T - T_\infty) = 0 \tag{6}$$

$$u\frac{\partial C}{\partial x} + v\frac{\partial C}{\partial y} = D_B\frac{\partial^2 C}{\partial y^2} + \frac{D_T}{T_\infty}\frac{\partial^2 T}{\partial y^2} \tag{7}$$

The associated boundary conditions are

$$\left.\begin{gathered} u = U_w(x) + L\frac{\partial u}{\partial y}, v = v_w, -k\frac{\partial T}{\partial y} = h_1(T_w - T), D_B\frac{\partial C}{\partial y} = h_2(C_w - C)\ at\ y = 0 \\ u \to 0, T \to T_\infty, C \to C_\infty\ as\ y \to \infty \end{gathered}\right\} \tag{8}$$

Where $U_w(x) = ax$, u and v represent velocity components in the x-and y-directions, λ is the time constant, $\tau\left(=\frac{(\rho c)_p}{(\rho c)_f}\right)$ is the ratio between the effective heat capacity of the nanoparticle material and heat capacity of the fluid, D_T for thermophoresis diffusion constant, D_B for Brownian diffusivity constant, T for temperature, C for Nanoparticle volume fraction, $\nu\left(=\frac{\mu}{\rho_f}\right)$ stands for kinematic viscosity, $\alpha\left(=\frac{k}{\rho c_p}\right)$ is the effective thermal diffusivity, k is the thermal conductivity of the fluid, ρ is the fluid density, c_p is the specific heat, $q_r = -\frac{16\sigma^* T^3}{3k^*}\frac{\partial T}{\partial y}$ is the radiative heat flux, k^* is the mean absorption coefficient, $\sigma^*$is the Stefan-Boltzmann constant, the term $Q_0(T - T_\infty)$ is assumed to be the amount of heat generated or absorbed per unit volume Q_0 as the coefficient constant, which may take on either positive or negative value. When the wall temperature T exceeds the free stream temperature T_∞, the source term $Q_0 > 0$ and heat sink when $Q_0 < 0$.

To converting the governing equations into ordinary differential equations, we introduce the following similarity transformations

$$\left.\begin{gathered} \psi = x\sqrt{a\nu}f(\eta), T = T_\infty\big(1 + (\theta_w - 1)\theta(\eta)\big), \eta = y\sqrt{\frac{a}{\nu}}, \\ \phi(\eta) = \frac{C - C_\infty}{C_m - C_\infty}. \end{gathered}\right\} \tag{9}$$

(With $\theta_w = \frac{T_m}{T_\infty}$ is the temperature difference parameter so that $T_m > T_\infty$)

By using above similarity transformations the equations (4) - (7) reduces to

$$f'''\left[1 + \left(\frac{n-1}{2}\right)\lambda_1(f'')^2\right] + 2\left[\left(\frac{n-1}{2}\right)\lambda_1(f'')^2\right]\left[1 + \left(\frac{n-3}{2}\right)\lambda_1(f'')^2\right] + ff'' - f'^2 - Mf' = 0 \tag{10}$$

$$(\{1 + Nr[1 + (\theta_w - 1)\theta]^3\}\theta')' + Pr(f\theta' + Nb\theta'\phi' + Nt\theta'^2) + Q\theta = 0 \tag{11}$$

$$\phi'' + LePrf\phi' + \frac{Nt}{Nb}\theta'' = 0 \tag{12}$$

and the boundary conditions (8) are reduces to

$$\left.\begin{gathered} f[0] = s,\ f'[0] = 1 + \gamma_1 f''(0),\ \theta'[0] = -\gamma_2(1 - \theta[0]), \phi'[0] = -\gamma_3(1 - \phi[0]), \\ f'[\infty] \to 0,\ \theta[\infty] \to 0,\ \phi[\infty] \to 0. \end{gathered}\right\} \tag{13}$$

Where prime denotes differentiation with respect to η. λ_1 is he material parameter, Pr is the Prandtl number, M is the magnetic parameter, Nt is the thermophoresis parameter, Nb is the Brownian motion parameter and Le for Lewis number, Nr is the radiation parameter, $\gamma_1, \gamma_2, \gamma_3$ are velocity, thermal and solutal slip parameters respectively and s is for mass transfer parameter with $s > 0$ for suction and $s < 0$ for injection.

These parameters are defined by

$$\left.\begin{gathered} Pr = \frac{\mu c_p}{k}, \lambda_1 = \lambda^2 a^2, Nb = \frac{\tau D_B(C_m - C_\infty)}{\nu}, M = \frac{\sigma}{\rho a}B_0^2, Nr = \frac{16\sigma^* T_\infty^3}{3kk^*}, s = -\frac{V_w}{\sqrt{\nu a}}, \\ Nt = \frac{\tau D_T(T_m - T_\infty)}{T_\infty \nu}, Le = \frac{\alpha}{D_B}, \gamma_1 = L\sqrt{\frac{a}{\nu}}, \gamma_2 = \frac{h_1}{k}\sqrt{\frac{\nu}{a}}, \gamma_3 = \frac{h_2}{D_B}\sqrt{\frac{\nu}{a}} \end{gathered}\right\} \tag{14}$$

Expressions for the local skin friction co-efficient C_{fx}, local Nusselt number Nu_x and local Sherwood number Sh_x are defined as,

$$C_{fx} = \frac{2\tau_w}{\rho U_m^2}, Nu_x = \frac{xq_w}{k_\infty(T_m - T_\infty)}, \; Sh_x = \frac{xq_m}{D_B(C_m - C_\infty)} \tag{15}$$

Where k_∞ is the thermal conductivity of the nanofluid, in which wall shear stress τ_w, q_w and q_m are the heat and mass flux, respectively given by

$$\left.\begin{aligned} \tau_w &= \eta_0 \left(\frac{\partial u}{\partial y} + \lambda^2 \left(\frac{n-1}{2}\right) \left(\frac{\partial u}{\partial y} \left(\frac{\partial u}{\partial x}\right)^2 + 3\frac{\partial v}{\partial x}\left(\frac{\partial u}{\partial y}\right)^2 \right) \right)_{y=0} \\ q_w &= -k_\infty \left(\frac{\partial T}{\partial y}\right)_{y=0} + (q_r)_w \\ q_m &= -D_B \left(\frac{\partial C}{\partial y}\right)_{y=0} \end{aligned}\right\} \tag{16}$$

Applying similarity transformations (8) for skin friction coefficient and Nusselt number and Sherwood number are converted to

$$\left.\begin{aligned} Re_x^{1/2} C_{fx} &= \left(1 + \lambda_1 \left(\frac{n-1}{2}\right)\right) f''(0), \\ Re_x^{-1/2} Nu_x &= -(1 + Nr\theta_w^3)\theta'(0), Re_x^{-\frac{1}{2}} Sh_x = -\phi'(0). \end{aligned}\right\} \tag{17}$$

Where $Re_x = \frac{U_m(x)x}{\nu}$ is local Reynolds number.

NUMERICAL RESULTS AND DISCUSSION

This section deals with the theoretical and graphical behaviour of different physical quantities which are involving in the present flow problem. The set of equations (10) - (12) are highly nonlinear and coupled hence it cannot be solved analytically. The dimensionless mathematical problems given in equations (10) - (12) subject to the boundary conditions (13) are obtained using the Runge-Kutta fourth order based on shooting technique. For the purpose of discussing to provide physical insight into the present problem, comprehensive numerical computations were carrying out for various values of the flow parameters which describe the flow characteristics and the results are illustrated graphically. For computational purposes, the reason of integration η is consider as 0 to η_∞ is equivalent to 5, where η_∞ corresponds to $\eta \to \infty$ which lies very well outside the momentum and thermal boundary layer.

To understand the influence of the physical flow parameters on the non-dimensional velocity, temperature and nanoparticle volume fraction profiles along with the skin friction coefficient, as well as local nusselt number and local sherwood number is present and discuss for different flow parameter values.

The influence of power law index(n) on velocity, temperature and nano particle volume fraction profiles are shown in Fig. 1(a)-1(c), respectively for both suction ($s > 0$) and injection($s < 0$) cases. It is clear from Figs that increasing in the power law index(n) rises the fluid velocity in both cases. The opposite trend is noticed for the temperature and nanoparticle volume fraction profiles in both cases. Fig. 2(a)-2(c) illustrated the effect of the velocity slip parameter(γ_1) on the velocity, temperature and nanoparticle volume fraction profiles respectively for both suction ($s > 0$) and injection ($s < 0$) cases. It is evident that the fluid velocity decreases for larger values of the velocity slip parameter(γ_1). It is also seen that increasing the values of velocity slip parameter(γ_1) enhances the temperature and nano particle volume fraction profiles for both cases.

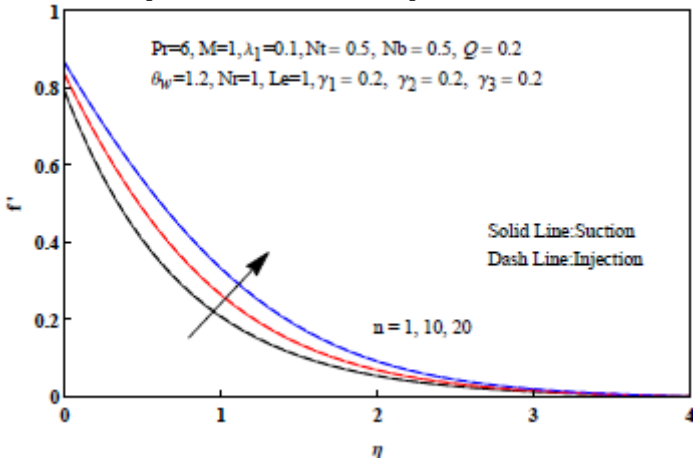

1(a) Velocity

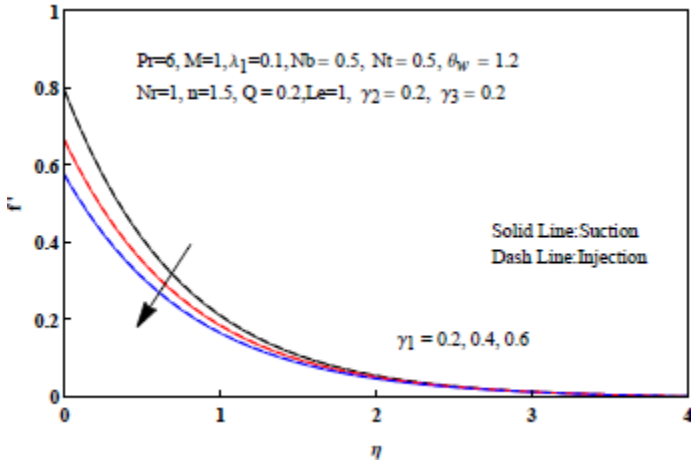

2(a) Velocity

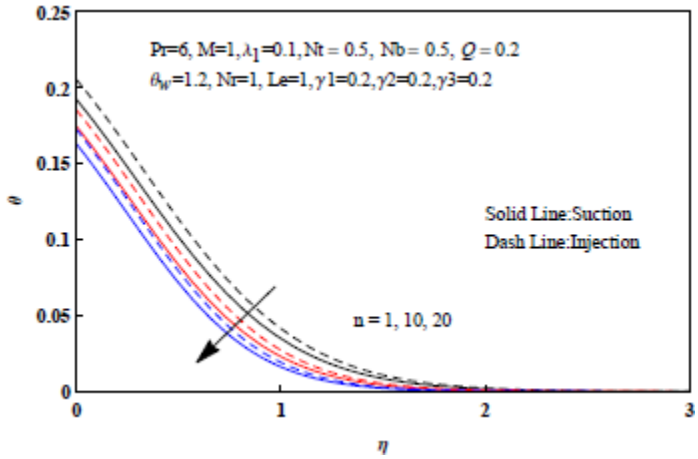

1(b) Temperature

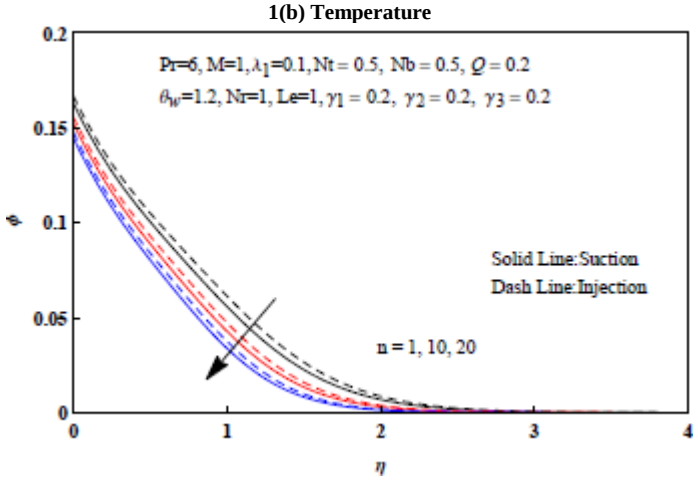

1(c) Nanoparticle volume fraction

Fig. 1 Variation of the Power law index *n* on Velocity, Temperature and Nanoparticle volume fraction profiles

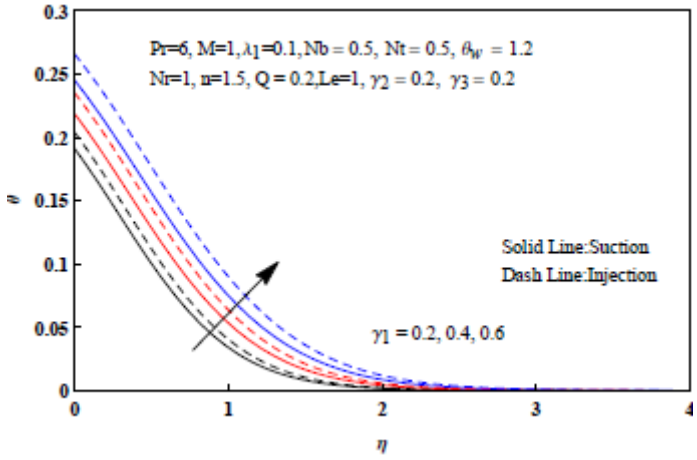

2(b) Temperature

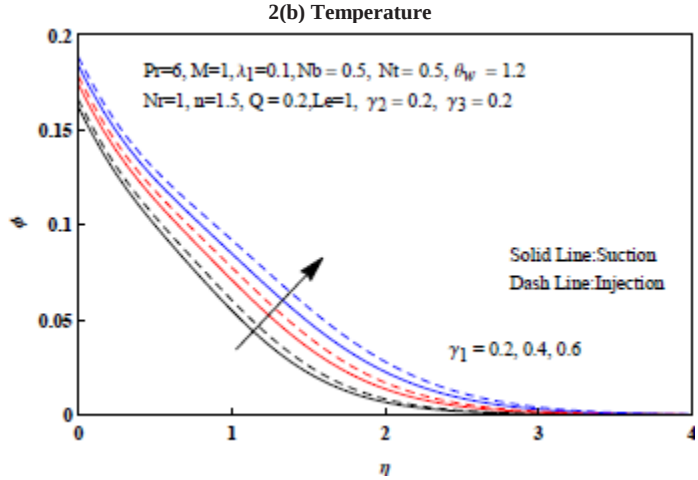

2(c) Nanoparticle volume fraction

Fig. 2 Variation of velocity slip parameter $\gamma_1$on Velocity, Temperature and Nanoparticle volume fraction profiles

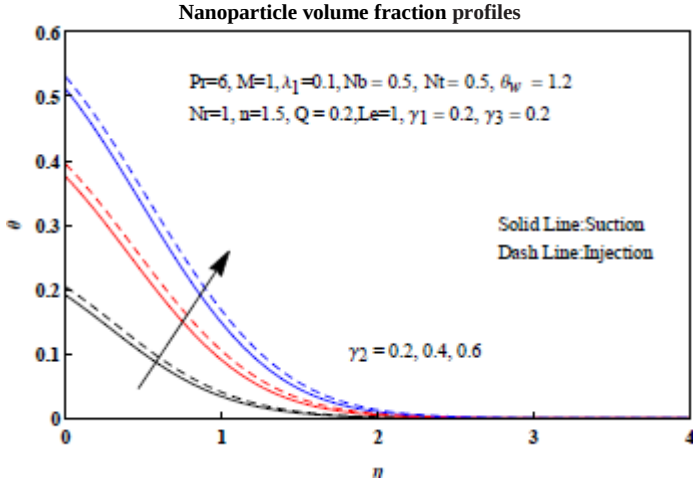

3(a) Temperature

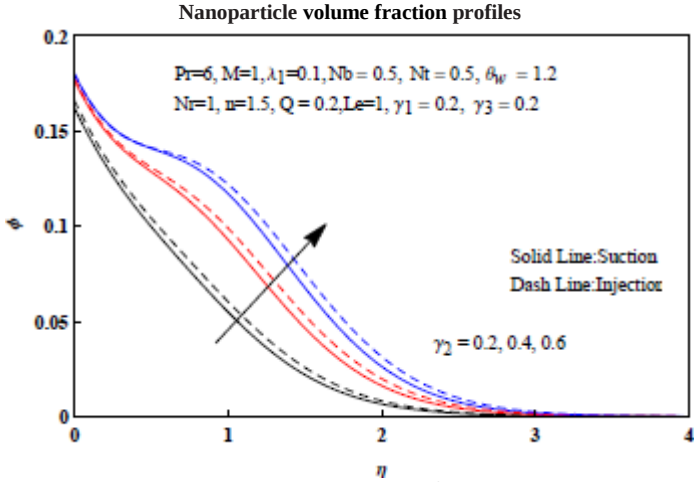

3(b) Nanoparticle volume fraction

Fig. 3 Variation of thermal slip parameter $\gamma_2$on Temperature and Nanoparticle volume fraction profiles

Figs 3(a)-3(b) &4(a)-4(b) present the effects of thermal and solutal slip parameters $(\gamma_2), (\gamma_3)$ on temperature and nanoparticle volume fraction profiles for both suction $(s > 0)$ and injection $(s < 0)$ cases respectively. It is observed that an increase in the values of thermal and solutal slip parameters is to enhances the temperature and nanoparticle volume fraction profiles for both cases.

Fig. (5) depicts the effect of material parameter(λ_1) on velocity profile for both suction $(s > 0)$ and injection $(s < 0)$ cases respectively. It is seen that by increasing the values of material parameter(λ_1) is to enhances the velocity profile in both cases. Fig. 6(a)-6(c) respectively, depicts for the influence of magnetic field parameter (M) on velocity, temperature and nanoparticle volume fraction for both suction $(s > 0)$ and injection $(s < 0)$ cases. It is notice that the impact of magnetic field is to reduce the velocity profile whereas enhances the temperature and nano-

particle volume fraction profiles for both cases. Physically as magnetic parameter (M) increases there is an increase in Lorentz forces, due to the influence of Lorentz force which provides resistance and opposes the flow. Consequently, the momentum boundary layer thickness is a decreasing function of the magnetic parameter (M), further the influence of magnetic field is decrease the momentum boundary layer thickness and enhances the thermal and nanoparticle boundary layer thickness.

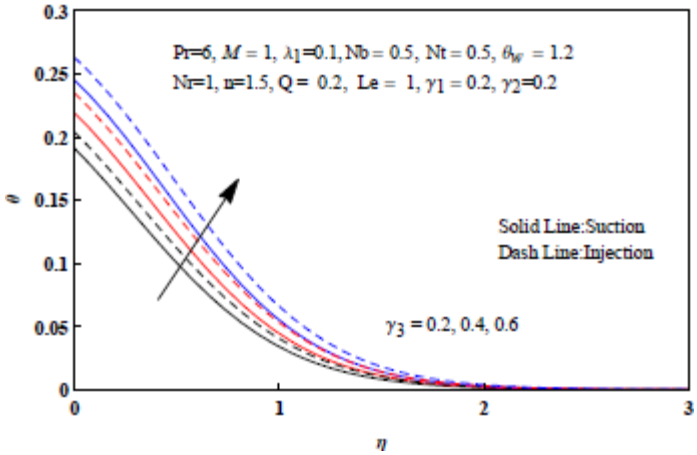

4(a) Temperature

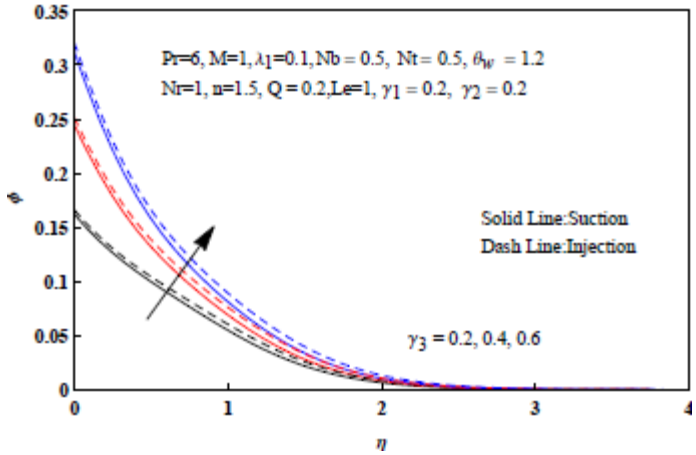

4(b) Nanoparticle volume fraction

Fig. 4 Variation of solutal slip parameter γ_3 on Temperature and Nanoparticle volume fraction profiles

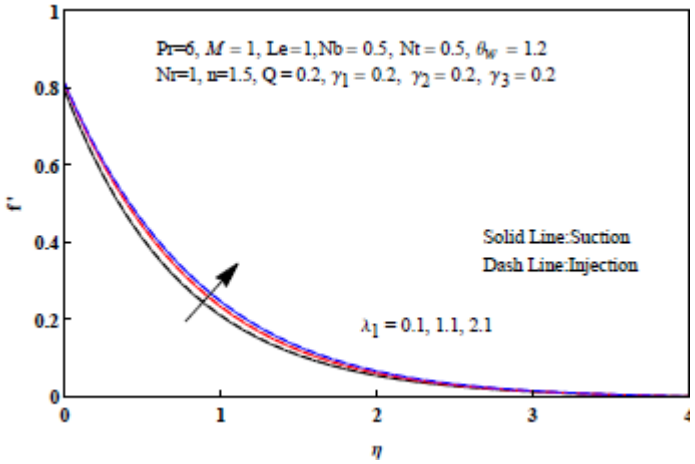

Fig. 5 Variation of the material parameter λ_1 on Velocity

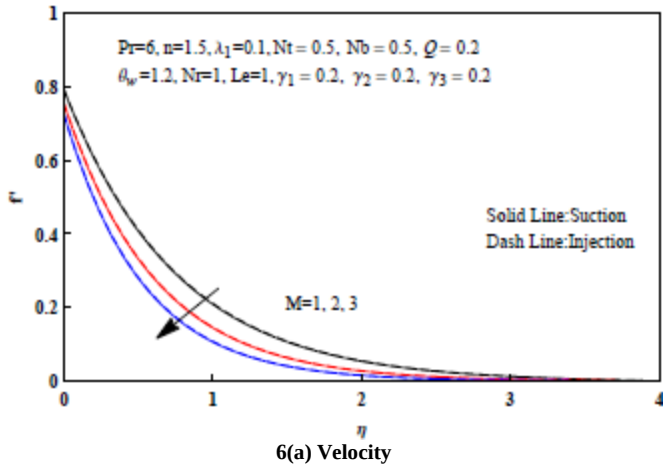

6(a) Velocity

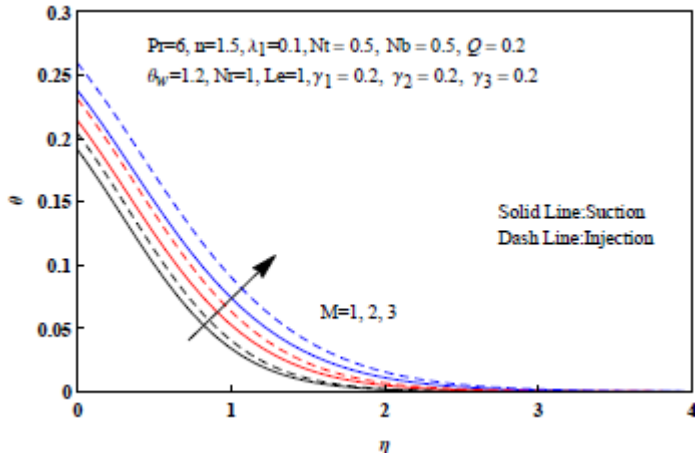

6(b) Temperature

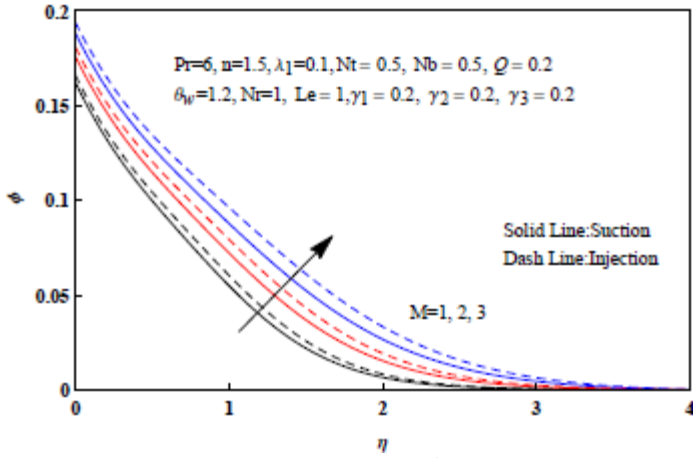

6(c) Nanoparticle volume fraction

Fig. 6 Variation of Magnetic field parameter M on Velocity, Temperature and Nanoparticle volume fraction profiles

Fig. 7 delineates the effect of nonlinear thermal radiation parameter (Nr) on temperature profile for both suction ($s > 0$) and injection ($s < 0$) cases respectively. It is observed that the temperature distribution and associated thermal boundary layer thickness increases for larger values of nonlinear thermal radiation parameter (Nr) in both cases. This is due to fact that the surface heat flux increases under the impact of nonlinear thermal radiation which

results in larger temperature inside the boundary layer region. Fig. 8(a)-8(b) discloses the effect of Prandtl number *(Pr)* on temperature and nanoparticle volume fraction profiles for both suction ($s > 0$) and injection ($s < 0$) cases, respectively. It is demonstrated through this Fig. that as increasing *Pr* is leading to decrease the temperature profiles as well as thermal boundary layer thickness in both cases. It is also seen that intensifying the Prandtl number decelerates the nanoparticle volume fraction profile and the associated concentration boundary layer in both cases. This is due to the fact that for small values of *Pr* are equivalent to larger values of thermal conductivities and therefore it is able to diffuse away from the stretching sheet.

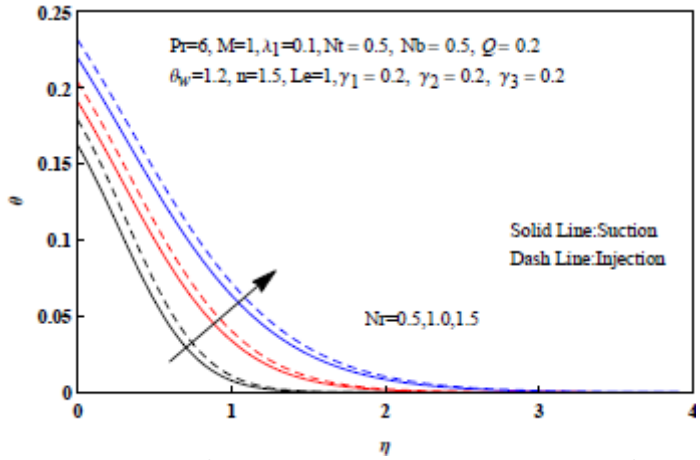

Fig. 7 Variation of Radiation parameter *Nr* on Temperature profile

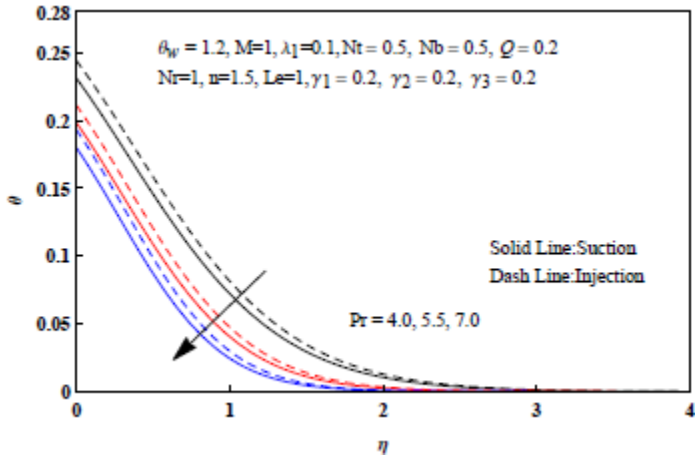

8(a) Temperature

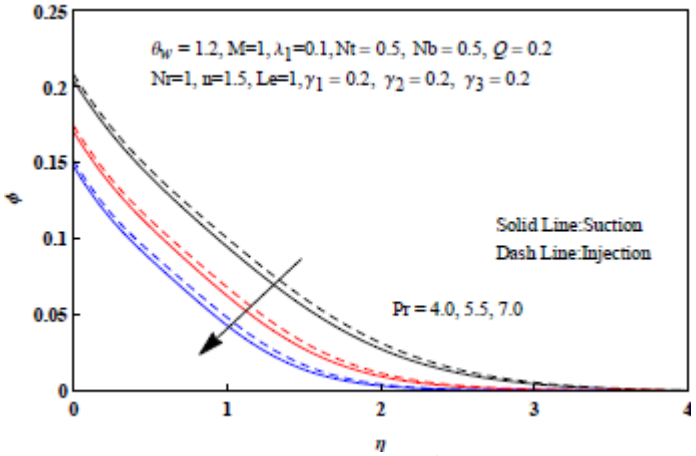

8(b) Nanoparticle volume fraction

Fig. 8 Variation of Prandtl number *Pr* on Temperature and Nanoparticle volume fraction profiles

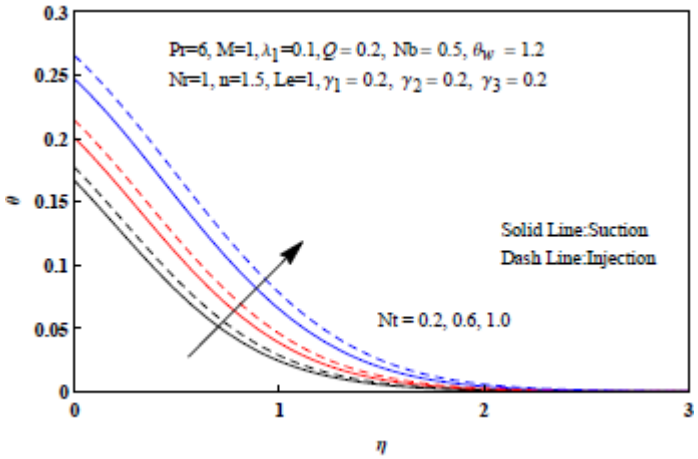

9(a) Temperature

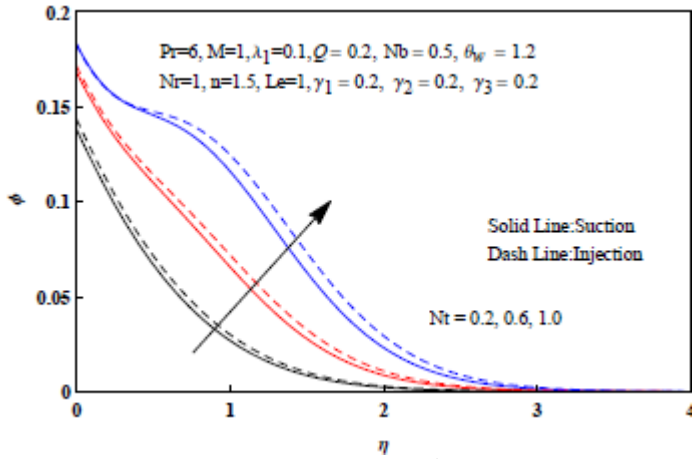

9(b) Nanoparticle volume fraction

Fig. 9 Variation of Thermophoresis parameter *Nt* on Temperature and Nanoparticle volume fraction profiles

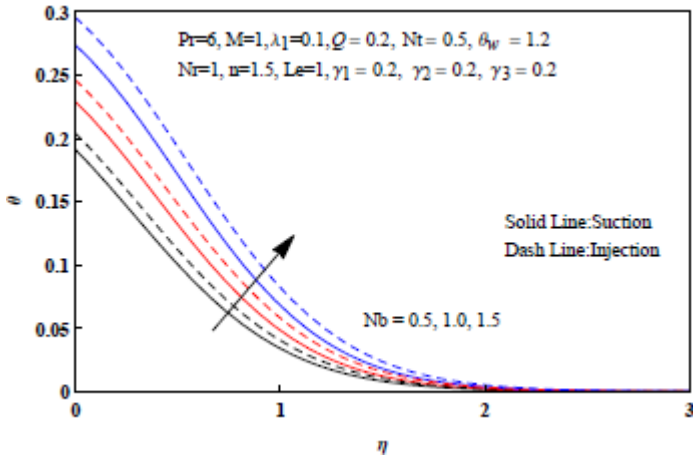

10(a) Temperature

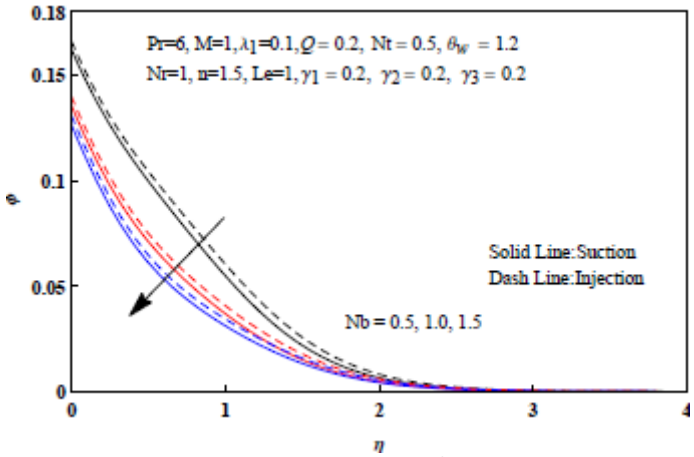

10(b) Nanoparticle volume fraction

Fig. 10 Variation of Brownian motion parameter *Nb* on temperature and Nanoparticle volume fraction profiles

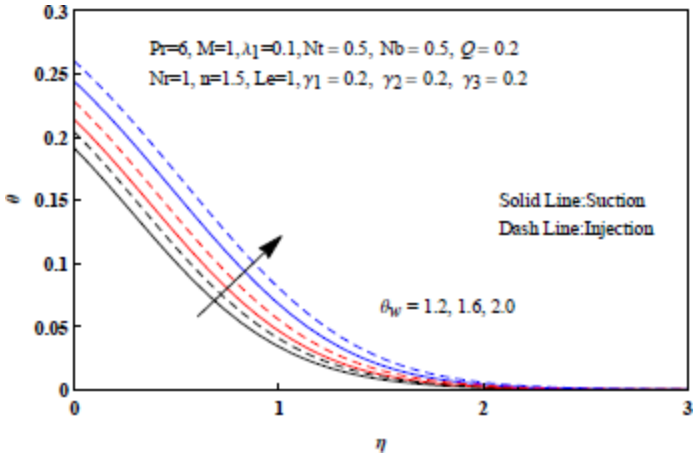

Fig. 11 Variation of temperature difference parameter θ_w on Temperature profile

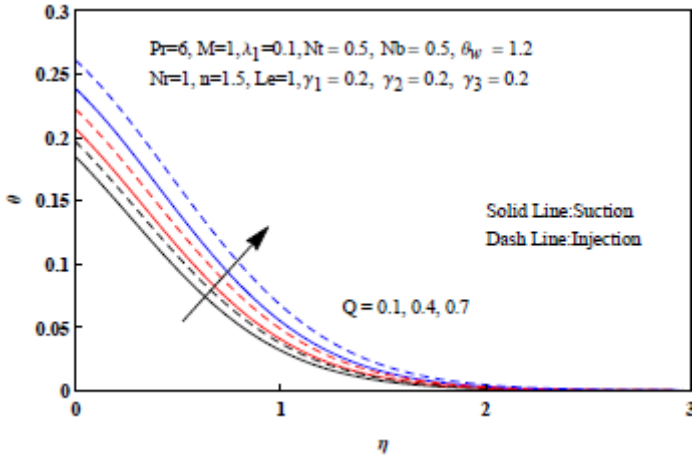

Fig. 12 Variation of heat source/sink parameter Q on Temperature profile

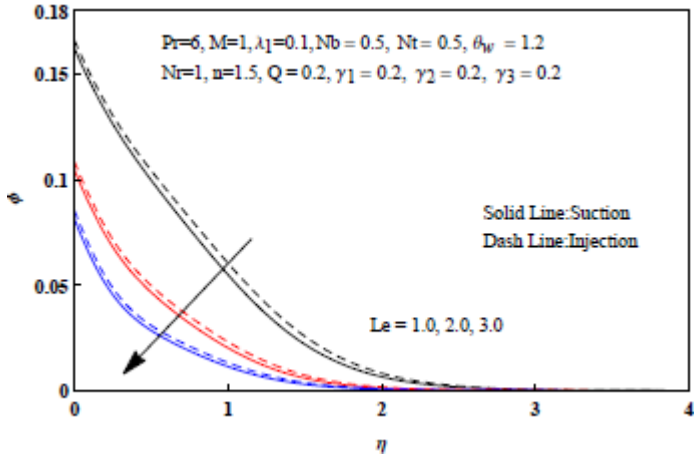

Fig. 13 Variation of Lewis number *Le* on Nanoparticle volume fraction profile

Fig. 9(a)-9(b) plotted the influence of Thermophoresis parameter *Nt* on temperature and nanoparticle volume fraction profiles respectively, for both suction ($s > 0$) and injection ($s < 0$) cases. Thermophoresis mechanism in which small particles are pulled away from hot surface to cold surface due to this the transportation temperature of the fluid arises. Therefore, the effect of thermophoresis parameter *Nt* is to enhances the temperature profiles in both cases. Physically, the thermophoresis force increments with the increase in the thermophoresis parameter which tends to move nanoparticles from hot to cold areas and hence increases the nanoparticle volume fraction profile. Fig. 10(a)-10(b) shows that the effect of Brownian motion parameter *Nb* on Temperature and nanoparticle volume fraction profiles for both suction ($s > 0$) and injection ($s < 0$) cases. It is observed that the temperature enhances by uplifting the Brownian motion parameter and it is also seen that the large values of Brownian motion parameter then decreases the nanoparticle volume fraction profile as well as concentration boundary layer thickness in both cases.

The influence of the temperature ratio parameter θ_w on the temperature profiles are depicted in Fig. (11) for both suction ($s > 0$) and injection ($s < 0$) cases respectively. From the Fig. it is clear that an enhancement in the temperature ratio parameter corresponds to higher wall temperature as compare to ambient fluid. As a consequence of that the temperature of the fluid arises in both cases. Moreover, we perceive that the thermal boundary layer thickness increases for large values of the temperature ratio parameter for both cases. Fig. (12) shows the effect of the heat source/sink parameter (Q) on the temperature profiles for both suction ($s > 0$) and injection ($s < 0$) cases respectively. The temperature profiles significantly increase as the heat source/sink parameter increases in both cases. Fig. (13) portray that the influence of Lewis number (Le) on nanoparticle volume fraction profiles for both suction ($s > 0$) and injection ($s < 0$) cases, respectively. It is observed from the Fig. that an increase in the values of Lewis number (Le) depreciates the nanoparticle volume fraction profile of the flow as well as concentration boundary layer thickness in both cases.

Table -1 is portrayed to indicate the influence of material parameter(λ_1), magnetic parameter (M), velocity slip parameter(γ_1) and power law index (n) on the local skin-friction coefficient for both suction ($s > 0$) and injection ($s < 0$) cases respectively. From this table, it is revealed that the local skin friction coefficient decreases by increasing the values of material parameter(λ_1), magnetic parameter (M) and power law index (n) for both suction($s > 0$) and injection($s < 0$) cases. The skin friction coefficient is an increasing function of velocity slip parameter in both cases.

Table -1 Numerical values of local skin friction coefficient $Re_x^{1/2}C_{fx}$ for various values of λ_1, M, γ_1 and n when pr=0.72, Nr=1, $\theta_w = 1.2$, Nb=0.1, Nt=0.1, Le=1, $\gamma_2 = \gamma_3 = 0.1$, Q=0.1

λ_1	M	γ_1	n	s=0.01	s=-0.01
0.2	0.5	0.1	1.5	−1.0769642	−1.0693711
0.4				−1.0985946	−1.0910103
0.6				−1.1241754	−1.1164972
0.2	0.5			−1.0769642	−1.0693711
	1.0			−1.2261880	−1.2188560
	1.5			−1.3530748	−1.3459733
	0.5	0.1		−1.0769642	−1.0693711
		0.2		−0.9570577	−0.9508117
		0.3		−0.8630009	−0.8577338
		0.1	1.5	−1.0769642	−1.0693711
			2.5	−1.1066607	−1.0993597
			3.5	−1.1320887	−1.1250871

Table -2 Numerical values of local Nusselt number $Re_x^{-1/2}Nu_x$ for various values of Nr, θ_w, Pr, Nt, Nb, Q when n=1.5, M=0.5, $\gamma_1 = 0.1$, Le=1, and $\lambda_1 = 0.2$

Nr	θ_w	Pr	Nt	Nb	Q	γ_2	s=0.01	s=-0.01
1.0	1.2	0.72	0.1	0.1	0.1	0.1	0.1958032	0.1939297
1.2							0.2153230	0.2134878
1.4							0.2355429	0.2337653
1.0	1.2						0.1958032	0.1939297
	1.4						0.2571375	0.2543595
	1.6						0.3317462	0.3278508
	1.2	0.72					0.1958032	0.1939297
		1.4					0.2284311	0.2270605
		2.1					0.2400758	0.2389569
		0.72	0.1				0.1958032	0.1939297
			0.3				0.1942447	0.1923142
			0.5				0.1926306	0.1906408
			0.1	0.1			0.1958032	0.1939297
				0.3			0.1946720	0.1927531
				0.5			0.1935239	0.1915590
				0.1	0.0		0.2288358	0.2283148
					0.2		0.2142357	0.2133236
					0.4		0.1790764	0.1769538
					0.1	0.1	0.1958032	0.1939297
						0.2	0.2938545	0.2893872
						0.3	0.3477758	0.3414253

Table -3 Numerical values of local Sherwood number – $\phi'(0)$ for various values of *Pr, Nt, Nb, Le,* γ_3 when *n=1.5, M=0.5,* $\lambda_1 = 0.2$,*Nr=1,* $\theta_w = 1.2, \gamma_1 = \gamma_2 = 0.1, Q = 0.1$

Pr	*Nt*	*Nb*	*Le*	γ_3	*s=0.01*	*s=-0.01*
0.72	0.1	0.1	1	0.1	0.0773865	0.0774423
1.4					0.0801620	0.0798948
2.1					0.0839110	0.0835954
0.72	0.1				0.0773865	0.0774423
	0.2				0.0738050	0.0742398
	0.3				0.0705344	0.0713654
	0.1	0.10			0.0773865	0.0774423
		0.15			0.0787160	0.0786532
		0.20			0.0793808	0.0792587
		0.1	1		0.0773865	0.0774423
			2		0.0842134	0.0841087
			3		0.0876279	0.0874744
			1	0.1	0.0773865	0.0774423
				0.2	0.1304725	0.1302373
				0.3	0.1691514	0.1685366

Table -2 is constructed to demonstrate the influence of the radiation parameter(*Nr)*, the temperature difference parameter(θ_w), the prandtl number(*Pr)*, the thermophoresis parameter (*Nt)*, the Brownian motion parameter (*Nb)*, the Lewis number(*Le)*, the heat source/sink parameter (*Q)* and the thermal slip parameter(γ_2) on the local Nusselt number for both suction ($s > 0$) and injection ($s < 0$) cases respectively. On the evident of table4, an enhancement in the radiation parameter, temperature difference parameter, thermal slip parameter and prandtl number grows the local Nusselt number both in suction and injection cases. It is also examined that the local Nusselt number is a decreasing function of the thermophoresis parameter, Brownian motion parameter and the heat source/sink parameter in both cases.

Table -3 provides a sample of our numerical results of the reduced Sherwood number for selected values of the Prandtl number, thermophoresis parameter, Brownian motion parameter, Lewis number and solutal parameter for both suction ($s > 0$) and injection ($s < 0$) cases, respectively. From this table, it can be seen that the local shearwood number enhances by uplifting the Prandtl number, Lewis number, Brownian motion parameter and solutal slip parameter in both cases. It is also noted that rise in thermophoresis parameter depreciate the mass transfer rate in both cases.

CONCLUSIONS

In this article, a numerical investigation is carried out for analysing the heat and mass transfer in carreau nanofluid flow over a permeable stretching sheet with convective boundary conditions in the presence of nonlinear thermal radiation, magnetic field, heat source\sink and suction\injection. The main conclusions have been summarized as follows:

- The dimensionless temperature and nanoparticle volume fraction profiles were dispirited as increasing of power law index for both suction and injection cases.
- The dimensionless temperature was enhanced for the higher values of nonlinear thermal radiation, temperature difference parameter and heat source/sink parameter for both suction and injection cases.
- The dimensionless temperature and nanoparticle volume fraction profiles were enhanced by uplifting velocity, thermal and solutal slip parameters in both suction and injection cases.
- The dimensionless velocity decreases for large values of magnetic field parameter and velocity slip parameter in both cases.
- It is found that larger values of thermophoresis parameter and Brownian motion parameter lead to increases in temperature profile for both suction and injection cases.
- The dimensionless nanoparticle volume fraction profiles decelerate as increasing in Brownian motion parameter, prandtl number and lewis number for both suction and injection cases. It is also seen that temperature profile is to decelerate by uplifting prandtl number in both cases.
- The skin friction coefficient decreases with the increase of magnetic field parameter, power law index and material parameter and it increases with the increase of velocity slip parameter.
- The local nusselt number increases by uplifting nonlinear thermal radiation, temperature difference parameter, prandtl number and it decreases with the increase of thermophoresis parameter, Brownian motion parameter and thermal slip parameter.

- The local Sherwood number increases with the larger values of prandtl number, Brownian motion parameter, lewis number and solutal slip parameter and it decreases with the increase of thermophoresis parameter.

Acknowledgements
This research was supported by University Grants Commission-India under Faculty Development Programme. The author gratefully acknowledges the support of UGC.

Nomenclature

x	distance along the surface	Re	local Reynolds number
y	distance normal to the surface	A_1	first Rivlin–Ericksen tensor
u	velocity component in $x-$direction	n	power law index
v	velocity component in $y-$direction	$B(t)$	time dependent magnetic field
V	velocity field	B_0	intensity of magnetic field
T	temperature field	ρ	density of fluid
C	concentration field	ν	kinematic viscosity
τ	Cauchy stress tensor	α_m	effective thermal diffusivity
p	pressure	U_m	stretching velocity
$\boldsymbol{I}$	identity tensor	T_m	surface temperature
μ_0	zero shear rate viscosity	C_m	surface nanoparticle concentration
μ_∞	infinite shear rate viscosity	V_m	mass fluid velocity
μ	apparent viscosity	T_∞	ambient fluid temperature
$\dot{\gamma}$	shear rate	C_∞	ambient fluid concentration
λ_1	time material constant	D_T	thermophoresis diffusion coefficient
η	local similarity variable	D_B	Brownian diffusion coefficient
f'	dimensionless velocity	k	thermal conductivity
θ	dimensionless temperature	c_p	specific heat capacity
ϕ	dimensionless concentration	a	constant
M	magnetic parameter	V_0	uniform suction/injection velocity
Pr	Prandtl number	Nt	thermophoresis parameter
s	mass transfer parameter	Nb	Brownian motion parameter
C_{fx}	local skin friction coefficient	Le	Lewis number
Nu_x	local Nusselt number	τ_w	wall shear stress
Sh_x	local Sherwood number	q_w	wall heat flux
q_r	radiative heat flux	q_m	wall mass flux
k^*	mean absorption parameter	θ_w	temperature difference parameter
σ^*	Stefan-Boltzmann constant	Nr	nonlinear thermal radiation parameter
		Q	heat source\sink parameter

REFERENCES

[1] SUS Choi, Enhancing Thermal Conductivity of Fluids with Nanoparticles, *ASME International Mechanical Engineering Congress & Exposition, USA*, **1995**, 99–105, FED 231/MD.
[2] J Buongiorno, Convective Transport in Nanofluids, *Journal of Heat Transfer*, **2006,** 128, 240–50.
[3] WA Khan and I Pop, Boundary-Layer Flow of a Nanofluid Past a Stretching Sheet, *International Journal of Heat Mass Transfer*,**2010**, 53, 2477–2483.
[4] OD Makinde and A Aziz, Boundary Layer Flow of a Nanofluid Past a Stretching Sheet with a Convective Boundary Condition, *International Journal of Thermal Sciences*,**2011**, 50, 1326–1332.
[5] M Turkyilmazoglu, Exact Analytical Solutions for Heat and Mass Transfer of MHD Slip Flow in Nanofluids, *Chemical Engineering Science*, **2012**, 84, 182–187.
[6] OD Makinde, WA Khan and ZH Khan, Buoyancy Effects on MHD Stagnation Point Flow and Heat Transfer of a Nanofluid Past a Convectively Heated Stretching/ Shrinking Sheet, *International Journal of Heat Mass Transfer*, **2013,** 62, 526–533.
[7] A Zeeshan, M Baig, R Ellahi and T Hayat, Flow of Viscous Nanofluid Between the Concentric Cylinders, *Journal of Computational and Theoretical Nanoscience*, **2014**, 11, 646–654.
[8] M Sheikholeslami, S Abelman and DD Ganji, Numerical simulation of MHD nanofluid flow and heat transfer considering viscous dissipation, *International Journal of Heat Mass Transfer*, **2014**, 79, 212–222.
[9] T Hayat, M Farooq and A Alsaedi, Thermal Radiation Effect in MHD Flow of Powell– Eyring Nanofluid Induced by a Stretching Cylinder, *Open Phys*, **2015**, 13, 188–197.

[10] FM Abbasi, SA Shehzad, T Hayat and B Ahmad, Doubly Stratified Mixed Convection Flow of Maxwell Nanofluid with Heat Generation/Absorption, *Journal of Magnetism and Magnetic Materials*, **2016**, 404, 159–165.
[11] T Hayat, S Asad, M Mustafa and A Alsaedi, Boundary Layer Flow of Carreau Fluid Over a Convectively Heated Stretching Sheet, Applied Mathematics and Computation, **2014**, 246, 12-22.
[12] Nasir Ali and Tasawar Hayat, Peristaltic Motion of a Carreau Fluid in an Asymmetric Channel, *Applied Mathematics and Computation*, **2007**, 193(2), 535–552.
[13] BI Olajuwon, Convection Heat and Mass Transfer in a Hydromagnetic Carreau Fluid Past a Vertical Porous Plate in Presence of Thermal Radiation and Thermal Diffusion, *Thermal science*, **2011**, 15, 241-252.
[14] M S Tshehla, The Flow of a Carreau Fluid Down an Incline with a Free Surface, *International* Journal *of the Physical Sciences*, **2011**, 6, 3896-3910.
[15] A Malvandi and DD Ganji, Magnetic Field Effect on Nanoparticles Migration and Heat Transfer of Water/Alumina Nanofluid in a Channel, *Journal of Magnetism and Magnetic Materials*, **2014**, 362, 172–179.
[16] V Nikiforov, Magnetic Induction Hyperthermia, *Journal of Russian Physics*, **2007**, 50(9), 913–924.
[17] M Sheikholeslami, M Hatami and DD Ganji, Analytical Investigation of MHD Nanofluid Flow in a Semi-Porous Channel, *Powder Technology*, **2013**, 246, 327-336.
[18] M Jashim, O Uddin, A Beg and AI MD Ismail, Mathematical Modeling of Radiative Hydromagnetic Thermosolute Nanofluid Convection Slip Flow in Saturated Porous Media, *Hindawi Publishing Corporation*, **2014,** pages-11.
[19] SR Pop, T Grosan and I Pop, Radiation Effects on the Flow Near the Stagnation Point of a Stretching Sheet, *Technische Mechanik*, **2004**, 25(2), 100–106.
[20] NS Akbar, S Nadeem, R Ul Haq and ZH Khan, Radiation Effects on MHD Stagnation Point Flow of Nano Fluid Towards a Stretching Surface with Convective Boundary Condition, *Chinese journal of Aeronautics*, **2013**, 26, 1389–1397.
[21] R Cortell, Effects of Viscous Dissipation and Radiation on the Thermal Boundary Layer Over a Non-Linearly Stretching Sheet, *Physics Letters A*, **2008**, 372, pp.631–636.
[22] T Hayat and M Qasim, Influence of Thermal Radiation and Joule Heating on MHD Flow of a Maxwell Fluid in the Presence of Thermophoresis, *International Journal of Heat Mass Transfer*, **2010**, 53, 4780–4788.
[23] BJ Gireesha, B Mahanthesh, RSR Gorla and PT Manjunatha, Thermal Radiation and Hall Effects on Boundary Layer Flow Past a Non-Isothermal Stretching Surface Embedded in Porous Medium with Non-Uniform Heat Source/Sink and Fluid-Particle Suspension, *Heat Mass Transfer*, **2016**, 52(4), 897–911.
[24] A Pantokratoras, T Fang, Sakiadis Flow with Nonlinear Rosseland Thermal Radiation, *Physica Scripta*, **2013**, 87, 015703(5 pages).
[25] R Cortell, Fluid Flow and Radiative Nonlinear Heat Transfer Over a Stretching Sheet, Journal of King Saud University-Science, **2014**, 26, 161–167.
[26] Macha Madhu, Naikoti Kishan, Ali J Chamkha, MHD flow of a non-Newtonian nanofluid over a non-linearly stretching sheet in the presence of thermal radiation with heat source/sink, *Engineering Computations*, 2016, 33(5),1610-1626.
[27] A Mushtaq, M Mustafa, T Hayat and A Alsaedi, Nonlinear Radiative Heat Transfer in the Flow of Nanofluid Due to Solar Energy: A Numerical Study, *Journal of Taiwan Institute of Chemical Engineers*, **2014**, 45, 1176–1183.
[28] Macha Madhu and Naikoti Kishan, MHD Boundary-Layer Flow of a Non-Newtonian Nanofluid Past a Stretching Sheet With a Heat Source/Sink, J*ournal of Applied Mechanics and Technical Physics*, **2016**, 57(5), 908–915.
[29] Hunegnaw Dessie and Naikoti Kishan, MHD Effects on Heat Transfer over Stretching Sheet Embedded in Porous Medium with Variable Viscosity, Viscous Dissipation and Heat Source/Sink, *Ain Shams Engineering Journal*, **2014**, 5, 967–977.
[30] Srinivas Maripala and Kishan Naikoti, MHD Effects on Micropolar Nanofluid Flow Over a Radiative Stretching Surface with Thermal Conductivity, *Advances in Applied Science Research*, **2016**, 7(3), 73-82.
[31] BJ Gireesha, B Mahanthesh and Rama Subba Reddy Gorla, Suspended Particle Effect on Nanofluid Boundary Layer Flow Past a Stretching Surface, *Journal of Nanofluids*, **2014**, 3(11), 267-277.
[32] EM Sparrow and RD Cess, Temperature-Dependent Heat Sources or Sinks in a Stagnation Point Flow, *Applied Scientific Research*, **1961**, 10(1), 185–197.
[33] MA Azim, AA Mamun and MM Rahman, Viscous Joule Heating MHD-Conjugate Heat Transfer for a Vertical Flat Plate in the Presence of Heat Generation, *International Communications in Heat and Mass Transfer*, **2010**, 37(6), 666–674.
[34] P Rana and R Bhargava, Numerical Study of Heat Transfer Enhancement in Mixed Convection Flow Along a Vertical Plate with Heat Source/Sink Utilizing Nanofluids, *Communications in Nonlinear Science and Numerical Simulation*, **2011**, 16(11), 4318–4334.
[35] MK Nayak, Chemical Reaction Effect on MHD Viscoelastic Fluid Over a Stretching Sheet Through Porous Medium, *Meccanica*, **2016**, 51, 1699–1711.
[36] T Hayat, M Imtiaz and A Alsaedi, MHD Flow of Nanofluid over Permeable Stretching Sheet with Convective Boundary Conditions, *Thermal Science*, **2016**, 20(6), 1835-1845.